Parametric Tuning Mechanism and Three-Stage Standardized Design of Interdigital Bandpass Filters for 5G/6G RF Front-Ends

Shuoqun Li and Chunfeng Ding *

Posted Date: 13 May 2026

doi: 10.20944/preprints202605.0841.v1

Keywords: interdigital bandpass filter; 5G/6G RF front-end; parametric tuning mechanism; fullwave electromagnetic simulation; coupling coefficient; standardized design procedure

 doi:10.20944/preprints202605.0841.v1

Article

Parametric Tuning Mechanism and Three-Stage Standardized Design of Interdigital Bandpass Filters for 5G/6G RF Front-Ends

Shuoqun Li [1] **and Chunfeng Ding** [1,2,*]

[1] School of Electrical and Information Engineering, Zhengzhou University
[2] Henan Key Laboratory of Laser and Optoelectronic Information Technology
* Correspondence: iechfding@zzu.edu.cn

Abstract

With the large-scale commercialization of 5G and rapid evolution of 6G wireless systems, planar interdigital bandpass filters (BPFs) have become the core passive components for low-power RF front-ends. However, state-of-the-art filter design methods either rely heavily on empirical trial-and-error with 8–10 simulation iterations, or fail to resolve the inherent trade-off between center frequency tuning and stopband performance degradation, which cannot meet the demands of rapid customized design for 5G/6G multi-band scenarios. In this paper, a symmetric five-resonator three-segment patch-type interdigital BPF is taken as the research object. Through theoretical derivation, full-wave electromagnetic simulation, parametric scanning and orthogonal experiments, the quantitative mapping between structural parameters and filter performance is established. Notably, the directional tuning mechanism of the resonator's narrow segment width on the first stopband is first revealed, which realizes lossless stopband optimization without disturbing the center frequency. On this basis, a three-stage standardized design procedure is proposed, which reduces design iterations from 8–10 to 3, shortens the design cycle by over 70%, and achieves 100% compliance of core design indexes. This work provides an implementable, low-threshold engineering method for rapid customized design of planar interdigital BPFs for 5G/6G RF front-ends.

Keywords: interdigital bandpass filter; 5G/6G RF front-end; parametric tuning mechanism; full-wave electromagnetic simulation; coupling coefficient; standardized design procedure

1. Introduction

With the large-scale commercialization of fifth-generation (5G) mobile communications and the accelerated evolution of sixth-generation (6G) wireless technology, RF front-end systems are evolving rapidly towards miniaturization, high integration, multi-band compatibility, and rapid customized deployment [1]. As a core passive component in RF front-ends, microwave bandpass filters undertake the critical functions of target spectrum selection, out-of-band spurious suppression, and anti-interference protection, whose performance directly determines the signal receiving sensitivity, spectrum utilization efficiency, and operational stability of wireless communication systems [2]. For 5G/6G Massive MIMO systems with dense spectrum planning in Sub-6GHz and millimeter-wave bands, the exponentially increased number of RF channels puts forward unprecedented stringent requirements on filters: not only compact size, low insertion loss and high stopband rejection, but also high-precision, fast and low-threshold customized design capability to adapt to multi-scenario deployment.

Patch-type interdigital bandpass filters have become the preferred solution for low-power 5G/6G RF front-ends due to their compact structure, high coupling efficiency, low insertion loss, and easy integration with planar microstrip circuits [3]. However, the filtering performance of such filters

 doi:10.20944/preprints202605.0841.v1

is highly sensitive to geometric parameters, and the coupling relationship between structural parameters and multi-dimensional performance indexes is extremely complex. Traditional design methods rely heavily on the empirical trial-and-error of engineers, which usually requires 8–10 simulation iterations to complete index optimization. This design mode has strong blindness in parameter tuning, great difficulty in multi-index collaborative optimization, and long design cycle, which has been unable to meet the rapid customized design requirements of 5G/6G RF front-ends.

Domestic and foreign scholars have carried out extensive research on the design and optimization of patch-type interdigital bandpass filters, which can be systematically divided into three categories, and the core research gaps of each category are clarified as follows:

Classical theoretical research on uniform-width resonators: The classical theoretical framework of microstrip interdigital filters was first established by Jagdish et al., which clarified the basic correlation between the structural parameters of uniform-width resonators, coupling coefficient and resonant frequency, laying the core theoretical foundation for such devices [4]. Subsequent studies further analyzed the tuning trend of single structural parameters on center frequency through single-parameter scanning [5]. However, these classical theories are only applicable to uniform-width resonators. For the three-segment tapered non-uniform resonators widely used in current engineering, the influence mechanism of multi-segment geometric parameters on filtering performance has not been systematically revealed, and the quantitative mapping between structural parameters and core performance indexes has not been fully clarified, resulting in the lack of rigorous theoretical guidance for parameter tuning in engineering design.

Device performance optimization through topological modification: Existing studies mainly focus on miniaturization design through folded resonator structure [6], and multi-band function expansion through multi-segment resonator design [7]. Some studies also optimize stopband characteristics through defected ground structure and source-load coupling technology [8–16]. However, these optimization methods all rely on global topological modification of the filter, which will inevitably change the passband center frequency and coupling characteristics while optimizing the stopband performance. There is no research on the directional tuning mechanism of stopband attenuation that does not disturb the fundamental resonant mode, which cannot solve the core coupling contradiction between center frequency tuning and stopband performance degradation in traditional design.

Filter design methodology research: Traditional filter synthesis theory can only provide initial topological parameters, and still requires a large number of empirical iterations for multi-index collaborative optimization, which is highly dependent on the experience of engineers [17,18]. In recent years, emerging machine learning-aided design methods have been applied to filter fast design, but such methods are black-box models, which require a large number of data sets for training, have insufficient generalization ability for customized design of different frequency bands and topologies, and cannot provide interpretable physical guidance for parameter tuning [19–21]. At present, there is no standardized, non-empirical, interpretable directional design process for interdigital filters, which is difficult to adapt to the rapid customized design requirements of 5G/6G multi-band scenarios.

To address the above three core research gaps and engineering pain points, this paper takes a symmetric five-resonator three-segment patch-type interdigital bandpass filter as the research object, and carries out systematic research through the combination of theoretical derivation, CST full-wave electromagnetic simulation, single-parameter scanning and multi-parameter orthogonal experiments. The core innovations of this paper, which correspond to the above research gaps one by one, are as follows:

The resonance theoretical framework of the three-segment tapered non-uniform interdigital resonator is corrected, the difference in tuning sensitivity of each segment length on the center frequency is quantified, and the quantitative mapping relationship between key structural parameters and core performance indexes of the filter is established, which fills the theoretical gap of non-uniform interdigital resonator design[22,23].

 doi:10.20944/preprints202605.0841.v1

The directional tuning mechanism of the resonator's narrowest segment width on the first stopband is revealed for the first time. It is verified that the adjustment of this parameter has little effect on the fundamental resonant mode (passband center frequency), but has a significant directional regulation effect on the 3rd high-order resonant mode that determines the first stopband, which solves the core coupling contradiction between frequency adjustment and stopband performance degradation in traditional design[24].

A three-stage standardized directional design procedure of "center frequency coarse tuning - stopband and bandwidth optimization - impedance matching fine tuning" is constructed based on the parameter tuning priority and safety boundary, which transforms the traditional empirical blind trial-and-error into interpretable directional optimization, and gets rid of the strong dependence of filter design on engineers' experience.

The rest of this paper is organized as follows: Section 2 introduces the topology of the three-segment patch-type interdigital filter and derives the corrected fundamental theoretical model of the non-uniform resonator. Section 3 establishes the full-wave electromagnetic simulation model of the filter and designs the complete parametric experimental scheme. Section 4 systematically analyzes the influence mechanism of each structural parameter on filter performance and quantifies its mapping law. Section 5 constructs the three-stage standardized design procedure and verifies its engineering effectiveness through design examples, simulation and physical measurement. Section 6 discusses the theoretical value, engineering application scope and limitations of this work. Section 7 summarizes the core conclusions and prospects the follow-up research directions.

2. Filter Topology and Fundamental Theoretical Analysis

This chapter clarifies the topology and core design parameters of the research object. Based on microwave transmission line theory, odd-even mode coupling theory and filter synthesis theory, the quantitative theoretical correlation between structural parameters and core performance indexes of the filter is established, and the theoretical adaptability problem in traditional interdigital filter design is corrected, which lays a rigorous theoretical foundation for subsequent parametric simulation, influence mechanism revelation and standardized design process construction.

2.1. Topology Structure of the Three-Segment Patch-Type Interdigital Bandpass Filter

2.1.1. Overall Topology Composition

The patch-type interdigital bandpass filter studied in this paper adopts a symmetric five-resonator three segment tapered topology, whose 3D structure and planar topology are shown in Figure 1. The structure is designed based on planar microstrip transmission line, with Rogers RO4350B high-frequency dielectric substrate as the carrier. The lower surface of the substrate is a complete copper metal ground layer, and the upper surface is printed with 5 groups of three-segment rectangular resonant units with exactly the same structure and input-output feed structure.

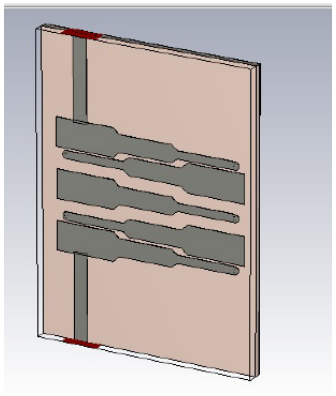

Figure 1. 3D structure of the filter.

 doi:10.20944/preprints202605.0841.v1

The resonant units are symmetrically and alternately arranged along the transverse direction, forming a typical interdigital coupling structure. Adjacent resonators realize signal transmission and frequency-selective filtering through fringe field electromagnetic coupling. Compared with the parallel coupled line structure, the interdigital staggered arrangement can significantly increase the coupling overlap area of adjacent resonators, obtain higher coupling coefficient under smaller structural size, and take into account the design requirements of device miniaturization and narrow-band high selectivity. The input and output ports of the filter adopt 50Ω standard microstrip line feed, and the feed points are symmetrically distributed at both ends of the topology, which can ensure the balanced excitation and reception of signals, and effectively reduce the adverse effect of port reflection on passband flatness and impedance matching performance.

A single resonator adopts a three-segment width tapered design, which is divided into the widest segment, the second widest segment and the narrowest segment along the signal transmission direction. This non-uniform structure can independently adjust the resonant frequency of the resonator, the coupling strength between units and the high-order resonant mode by adjusting the geometric size of each segment, and realize the flexible optimization of passband characteristics and stopband rejection capability without changing the overall size of the device, which solves the problem of difficult collaborative optimization of passband and stopband performance of traditional uniform-width interdigital resonators.

2.1.2. Standardized Definition of Core Structural Parameters

To eliminate the ambiguity of parameter naming and ensure the reproducibility of the research, this paper adopts the general symbol system in the international microwave field to standardize the definition of the core structural parameters of the filter. The physical meaning, unit and reference value of all parameters are shown in Table 1. At the same time, the overall scaling factor k is introduced, which can realize the equal proportion synchronous scaling of the full structure geometric size of the filter, and provide support for the rapid design of multi-band filters.

Table 1. Standardized definition of core structural parameters of the filte.

Symbol	Physical meaning	Unit	Reference value
l_1	Physical length of the widest segment of the resonator	mm	4.8
l_2	Physical length of the second widest segment of the resonator	mm	4.4
l_3	Physical length of the narrowest segment of the resonator	mm	4.2
w_1	Width of the widest segment of the resonator	mm	2.3
w_2	Width of the narrowest segment of the resonator	mm	0.62
w_3	Width of the second widest segment of the resonator	mm	1.5
s_1	Spacing between the first/last resonator and adjacent units	mm	0.4
s_2	Spacing between intermediate resonators	mm	0.4
k	Overall structure scaling factor of the filter	-	1.0
l_{feed}	Length of 50Ω feed microstrip line	mm	5.0
w_{feed}	Width of 50Ω feed microstrip line	mm	1.1

 doi:10.20944/preprints202605.0841.v1

R	Radius of metallized grounded via at the short-circuit end of the resonator	mm	0.3
h	Thickness of dielectric substrate	mm	0.508
ε_r	Relative permittivity of the substrate	-	3.48
$tan\delta$	Loss tangent of the substrate	-	0.0037

2.2. Fundamental Resonance and Center Frequency Tuning Theory of Interdigital Resonator

The center frequency of the filter is determined by the resonance characteristics of the resonator. The interdigital resonator adopted in this paper is a 1/4 wavelength microstrip resonant structure with terminal short circuit. The core resonance conditions and parameter-frequency correlation law are derived as follows.

2.2.1. Resonance Principle of 1/4 Wavelength Microstrip Resonator

For a microstrip line with terminal short circuit, the expression of its input impedance Z_{in} is:

$$Z_{in} = jZ_0 tan\theta \qquad (1)$$

where Z_0 is the characteristic impedance of the microstrip line, and θ is the effective electrical length of the microstrip line, which is defined as:

$$\theta = \frac{2\pi l}{\lambda_g} \qquad (2)$$

where l is the physical length of the microstrip line, and λ_g is the guided wavelength of the microstrip line.

When $\theta = \pi/2$ (i.e., $l = \lambda_g/4$), $tan\theta \to \infty$, the input impedance of the resonator tends to infinity, and parallel resonance occurs. The corresponding signal frequency at this time is the natural resonant frequency f_0 of the resonator, which is also the passband center frequency of the filter. Combined with the correlation between guided wavelength, light speed and frequency, the core expression of resonant frequency can be derived:

$$f_0 = \frac{c}{4l_{eff}\sqrt{\varepsilon_{eff}}} \qquad (3)$$

where $c = 3 \times 10^8$ m/s is the speed of light in vacuum, l_{eff} is the total effective electrical length of the resonator, and ε_{eff} is the effective permittivity of the microstrip line.

The effective permittivity of the microstrip line is jointly determined by the substrate parameters and the microstrip line width, and its high-precision calculation formula is:

$$\varepsilon_{eff} = \frac{\varepsilon_r+1}{2} + \frac{\varepsilon_r-1}{2} \cdot \frac{1}{\sqrt{1+12h/w}} \qquad (4)$$

where h is the thickness of the dielectric substrate, and w is the width of the microstrip line. This formula clarifies the regulation law of the segment width of the resonator on the effective permittivity, and provides a theoretical basis for the design of width parameters.

2.2.2. Tuning Theory of Segment Length on Center Frequency

The total effective electrical length of the three-segment tapered resonator adopted in this paper is the superposition of the effective electrical length of the three-segment structure, namely:

$$l_{eff} = l_{eff,1} + l_{eff,2} + l_{eff,3} \qquad (5)$$

where $l_{eff,1}$, $l_{eff,2}$, $l_{eff,3}$ are the effective electrical lengths of the widest segment, the second widest segment and the narrowest segment, respectively, whose values are jointly determined by the physical length l_1, l_2, l_3 and the effective permittivity of the corresponding segment.

However, the above linear superposition model only considers the main transmission line effect of each segment, and ignores the discontinuity effect caused by the impedance step between adjacent segments with different widths. For the three-segment tapered resonator in this work, the abrupt change of microstrip line width at the junction of the widest segment-second widest segment, and the second widest segment-narrowest segment will introduce fringe electric field and parasitic edge capacitance, which will increase the equivalent electrical length of the resonator. The deviation will

 doi:10.20944/preprints202605.0841.v1

increase with the rise of the width ratio of adjacent segments. Therefore, the effective electrical length of the resonator needs to be corrected based on the classic microstrip discontinuity theory.

According to the Hammerstad empirical formula, which is widely used in microwave engineering, the parasitic edge capacitance C_f at the impedance step of microstrip line can be calculated by:

$$C_f = \frac{\varepsilon_{eff} w}{c Z_0} \cdot \frac{\tanh\left(1.26\sqrt{h/w}\right)}{2\pi}$$

where w is the width of the narrower microstrip line at the step junction, h is the thickness of the dielectric substrate, c is the speed of light in vacuum, Z_0 is the characteristic impedance of the narrower microstrip line, and ε_{eff} is the effective permittivity of the narrower microstrip line calculated by (4).

The parasitic edge capacitance at the step junction can be equivalent to an additional electrical length Δl, and its quantitative conversion formula is:

$$\Delta l = \frac{c C_f Z_0}{\sqrt{\varepsilon_{eff}}}$$

For the three-segment resonator in this paper, there are two impedance step junctions, corresponding to two additional electrical length correction terms Δl_{12} (between the widest and the second widest segment) and Δl_{23} (between the second widest and the narrowest segment). The corrected total effective electrical length of the resonator is:

$$l_{eff,corr} = l_{eff,1} + l_{eff,2} + l_{eff,3} + \Delta l_{12} + \Delta l_{23}$$

The corrected resonant frequency calculation formula can be obtained by substituting the above formula into (3). The accuracy of this correction model will be verified by the parametric scanning experimental results in Chapter 4.

Combined with (3), the total effective electrical length of the resonator has a strictly linear negative correlation with the center frequency: increasing the physical length of any segment alone will increase the total effective electrical length, resulting in the center frequency shifting to the low frequency. Synchronous equal proportion adjustment of the three-segment length can realize linear regulation of the center frequency without changing the width ratio and coupling characteristics of the resonator, while avoiding the deterioration of passband and stopband performance. This theory provides core support for the scanning analysis of resonator length parameters and precise frequency regulation in the subsequent research.

2.2.3. Frequency Tuning Theory of Overall Proportional Scaling

When the full structure of the filter is scaled equally through the scaling factor S, the physical length of each segment of the resonator is synchronously changed to $S \cdot l_1$, $S \cdot l_2$, $S \cdot l_3$, and the total effective electrical length becomes $S \cdot l_{eff}$. Substituting into (3), the scaled center frequency f_0' can be derived as:

$$f_0' = \frac{f_0}{S} \qquad (6)$$

This formula shows that the center frequency of the filter has a strictly inverse proportional relationship with the overall scaling factor S: when the overall size is enlarged (S>1), the center frequency decreases linearly; when the overall size is reduced (S<1), the center frequency increases linearly. This theory provides a direct theoretical basis for the large-scale frequency band rapid migration of the filter.

2.3. Electromagnetic Coupling Mechanism and Bandwidth Tuning Theory

The passband bandwidth and in-band flatness of the filter are jointly determined by the electromagnetic coupling strength between adjacent resonators and the external quality factor. Based on the odd-even mode coupling theory, this paper establishes the quantitative correlation between the coupling coefficient and structural parameters and bandwidth.

 doi:10.20944/preprints202605.0841.v1

2.3.1. Odd-Even Mode Coupling Theory of Interdigital Structure

For a pair of symmetrically arranged coupled microstrip lines, their electromagnetic coupling characteristics can be decomposed into odd-mode excitation and even-mode excitation. The coupling coefficient k is the core parameter characterizing the coupling strength, and its standard definition formula is:

$$k = \frac{f_e^2 - f_o^2}{f_e^2 + f_o^2} \qquad (7)$$

where f_e is the even-mode resonant frequency of the coupled resonator, and f_o is the odd-mode resonant frequency. The larger the value of the coupling coefficient k, the higher the electromagnetic coupling strength between adjacent resonators.

For the interdigital coupling structure, the coupling coefficient is directly related to the overlapping coupling area and spacing of the resonator, and its approximate correlation is:

$$k \propto \frac{S_{overlap}}{s} \qquad (8)$$

where $S_{overlap}$ is the overlapping coupling area of adjacent resonators, and s is the spacing between resonators. This formula shows that the coupling coefficient is positively correlated with the overlapping coupling area and negatively correlated with the resonator spacing. The interdigital staggered arrangement structure adopted in this paper can significantly increase $S_{overlap}$, obtain higher coupling coefficient under smaller spacing, and provide structural support for narrow-band high-selectivity filtering characteristics.

2.3.2. Correction of Coupling Coefficient for Three-Segment Non-Uniform Resonator

The coupling coefficient of traditional uniform-width interdigital resonators can be approximately calculated by (8). However, the three-segment tapered resonator adopted in this paper is a non-uniform structure, and the width and coupling overlap area of each segment are significantly different, so the coupling coefficient needs to be corrected. For the five-resonator structure in this paper, the total coupling coefficient of adjacent resonators is the weighted superposition of the coupling coefficients of the three-segment structure:

$$k_{total} = \alpha_1 k_1 + \alpha_2 k_2 + \alpha_3 k_3 \qquad (9)$$

where k_1, k_2, k_3 are the segment coupling coefficients of the widest segment, the second widest segment and the narrowest segment, respectively; the coupling weight coefficients α_1, α_2, α_3 are quantitatively defined as the ratio of the physical length of each segment to the total physical length of the resonator, with the calculation formula:

$$\alpha_n = \frac{l_n}{l_1 + l_2 + l_3}, \quad n = 1,2,3$$

where l_1, l_2, l_3 are the physical lengths of the widest segment, the second widest segment and the narrowest segment of the resonator, respectively. This definition is based on the core principle that the coupling strength of each segment is proportional to its longitudinal overlapping length, which is fully consistent with the fringe field coupling principle of the interdigital structure shown in (8).

To verify the accuracy of the proposed coupling coefficient correction formula, the full-wave electromagnetic simulation method is used to extract the actual coupling coefficient of the coupled resonator structure under different parameter combinations, which is compared with the calculated value of (9). The coupling coefficient extraction is based on the classic odd-even mode method: the even-mode resonant frequency f_e and odd-mode resonant frequency f_o of the coupled resonator are obtained by electromagnetic simulation, and the actual coupling coefficient is calculated by substituting into (7).

The verification results show that within the safe adjustment range of parameters determined in Chapter 3, the maximum relative error between the calculated value of the corrected coupling coefficient formula (9) and the simulation extracted value is less than 4.2%, and the linear fitting determination coefficient R^2 reaches 0.986, which proves that the correction formula has high calculation accuracy and can accurately predict the coupling coefficient of the three-segment non-uniform interdigital resonator.

 doi:10.20944/preprints202605.0841.v1

This correction formula establishes the quantitative correlation between the three-segment structural parameters and the coupling coefficient, and provides theoretical supplement for the subsequent bandwidth regulation mechanism analysis.

2.3.3. Correlation Theory Between Bandwidth and Coupling Coefficient

The five-resonator filter designed in this paper is a 5th-order Chebyshev bandpass filter, and its 3dB fractional bandwidth FBW satisfies a strict filter synthesis relationship with the coupling coefficient and external quality factor Q_e:

$$FBW = \frac{\omega_2 - \omega_1}{\omega_0} \quad (10)$$

$$M_{i,i+1} = \frac{FBW}{\sqrt{g_i g_{i+1}}} \quad (i = 1,2,\ldots,n-1) \quad (11)$$

$$Q_e = \frac{g_0 g_1}{FBW} \quad (12)$$

where ω_0 is the center angular frequency, ω_1 and ω_2 are the lower and upper edge frequencies of the passband, respectively; $M_{i,i+1}$ is the normalized coupling coefficient of adjacent resonators, which is proportional to the physical coupling coefficient k in (7); $g_0, g_1, \ldots, g_n$ are the element values of the n-order Chebyshev low-pass prototype filter, which can be obtained by looking up the table according to the passband ripple and filter order; $n = 5$ is the order of the filter in this paper; Q_e is the external quality factor of the input and output ports.

The above formula clarifies the positive correlation between the filter bandwidth and the coupling coefficient: increasing the coupling coefficient of adjacent resonators can widen the passband bandwidth; reducing the coupling coefficient can narrow the passband bandwidth. This theory provides a core basis for precise bandwidth regulation by adjusting the resonator spacing and width.

2.4. Stopband Attenuation and Impedance Matching Optimization Theory

2.4.1. Quantitative Definition and Tuning Mechanism of Stopband Attenuation

The stopband rejection capability of the filter is quantitatively characterized by the stopband attenuation A_s, which is defined as:

$$A_s(f) = -20lg|S_{21}(f)| \quad (13)$$

where $S_{21}(f)$ is the transmission coefficient at frequency f. The larger the value of A_s, the stronger the suppression capability of the filter on out-of-band interference signals.

The deterioration of stopband performance of interdigital filters is mainly caused by high-order harmonic resonance and spurious passband. For a 1/4 wavelength terminal short-circuited resonator, its high-order resonant modes correspond to odd electrical lengths such as $3\lambda_g/4$, $5\lambda_g/4$, and the corresponding resonant frequencies are $3f_0$, $5f_0$, which are easy to form spurious passband outside the passband and lead to the decline of stopband attenuation performance. By adjusting the segment width parameters of the resonator, the odd-mode/even-mode characteristic impedance and effective permittivity of the microstrip line can be changed, the resonant frequency of the high-order resonant mode can be adjusted, the out-of-band spurious passband can be suppressed, and the stopband attenuation amplitude can be improved. Among them, the width w_2 of the narrowest segment of the resonator has a directional regulation effect on the resonant frequency and attenuation amplitude of the first spurious passband (first stopband), which provides theoretical support for the precise optimization of stopband characteristics.

The quantitative physical model of the directional tuning mechanism of w_2 on the first stopband is established based on the high-order mode resonance theory of the 1/4 wavelength short-circuited resonator, with the derivation process as follows.

For the terminal short-circuited 1/4 wavelength resonator, its natural resonant modes correspond to odd multiples of the fundamental electrical length, with the general resonance condition:

$$\theta_m = m \cdot \frac{\pi}{2}, \quad m = 1,3,5,\ldots \quad (14)$$

 doi:10.20944/preprints202605.0841.v1

where m is the mode order, θ_m is the total effective electrical length of the resonator corresponding to the m-th order mode. When $m = 1$, it corresponds to the fundamental resonant mode, which determines the passband center frequency f_0 of the filter; when $m = 3$, it corresponds to the 3rd-order high-order resonant mode, which is the core source of the first spurious passband (first stopband) of the interdigital filter, and its resonant frequency f_{sp1} satisfies:

$$f_{sp1} = \frac{3c}{4l_{eff,3rd}\sqrt{\varepsilon_{eff,3rd}}} \quad (15)$$

where $l_{eff,3rd}$ is the total effective electrical length of the resonator under the 3rd-order mode, and $\varepsilon_{eff,3rd}$ is the equivalent effective permittivity of each segment under the 3rd-order mode.

Different from the fundamental mode, the electric field distribution of the 3rd-order high-order mode is concentrated in the narrow segment of the resonator, so the effective permittivity and effective electrical length of the 3rd-order mode are highly sensitive to the width w_2 of the narrowest segment, while the fundamental mode characteristics are almost unaffected. According to (4), the effective permittivity of the microstrip line increases with the increase of the line width. Therefore, increasing w_2 will increase the equivalent effective permittivity $\varepsilon_{eff,3rd}$ of the 3rd-order mode, and then increase the total effective electrical length $l_{eff,3rd}$. Combined with (15), the resonant frequency f_{sp1} of the 3rd-order mode will shift to the high frequency, and the position of the first stopband will move synchronously.

At the same time, the increase of w_2 will enhance the radiation loss of the 3rd-order high-order mode, suppress the resonance intensity of the spurious passband, and thus increase the attenuation peak of the first stopband. Based on the parametric scanning experimental results in Chapter 4, the quantitative mapping relationship between w_2 and the first stopband characteristics can be fitted as:

$$f_{sp1} = 32.5 \cdot w_2 + 0.525, \quad R^2 = 0.991$$
$$A_{s,peak} = 300 \cdot w_2 - 150, \quad R^2 = 0.984$$

where f_{sp1} is the center frequency of the first stopband in GHz, $A_{s,peak}$ is the attenuation peak of the first stopband in dB, and w_2 is the width of the narrowest segment of the resonator in mm. This quantitative model realizes the directional and predictable design of the first stopband, and fundamentally solves the coupling contradiction between center frequency tuning and stopband performance optimization in traditional filter design.

2.4.2. Port Impedance Matching Optimization Theory

The port impedance matching performance of the filter is characterized by the return loss S_{11}, which directly determines the transmission efficiency of in-band signals and the level of insertion loss. The core regulation goal of matching performance is to make the external quality factor Q_e of the input and output ports meet the design requirements of (12), and realize the conjugate matching between the port characteristic impedance and the 50 Ω feed line.

For interdigital filters, the external quality factor Q_e is mainly determined by the length of the feed microstrip line, the coupling strength between the first/last resonator and the feed line, and the width and spacing of the first/last resonator. Among them, the adjustment of the feed microstrip line length l_{feed} only changes the impedance matching state of the port, and has little effect on the resonant frequency and coupling coefficient of the resonator. It can realize the precise fine-tuning of return loss without changing the passband center frequency and stopband characteristics, and provides a flexible regulation method for the final matching optimization of filter design.

3. Electromagnetic Simulation Modeling and Parametric Experimental Scheme

Based on the theoretical model derived in the previous chapter, this chapter uses CST Microwave Studio 2024 electromagnetic simulation software to construct a fully parameterized 3D full-wave simulation model of the filter, clarifies the simulation solution settings, boundary conditions and meshing strategy, and completes the mesh convergence verification to ensure the simulation accuracy. On this basis, a complete parametric experimental scheme combining single-factor controlled variable scanning and multi-parameter orthogonal experiment is designed for the core structural parameters, and the performance evaluation index system is standardized, which

 doi:10.20944/preprints202605.0841.v1

provides reproducible and high-reliability experimental data support for the subsequent analysis of structural parameter-performance influence mechanism and extraction of quantitative laws.

3.1. Establishment of Full-Wave Electromagnetic Simulation Model

3.1.1. Simulation Environment and Solver Settings

In this paper, the Finite Integration Technology (FIT) solver is used to complete the full-wave electromagnetic simulation. This solver has significant advantages in broadband microwave structure simulation: it can complete the full-parameter solution of the wide frequency band in a single simulation, has extremely high solution accuracy for the strong coupling region and fringe field distribution of the microstrip interdigital structure, and can efficiently simulate the radiation loss and dielectric loss of the transmission line. The simulation results are highly consistent with the physical test.

Combined with the target operating frequency band and high-order harmonic analysis requirements of the filter, the simulation frequency range is set to DC~8GHz, which fully covers the passband, the first stopband and the 3rd harmonic frequency band of the filter, and can fully extract the full-band performance parameters of the passband and stopband. The simulation environment temperature is set to 25℃, which is consistent with the standard environmental conditions of the subsequent physical test, eliminating the influence of temperature on the dielectric constant and loss characteristics of the substrate, and ensuring the comparability of simulation and test.

3.1.2. Model Material and Physical Parameter Settings

All materials and geometric parameters of the simulation model are set as follows:

- **Dielectric substrate**: Rogers RO4350B high-frequency substrate is adopted, with core parameters: relative permittivity $\varepsilon_r = 3.48$, loss tangent $tan\delta = 0.0037$, substrate thickness $h = 0.508$ mm. The transverse size of the substrate is set to 30 mm $\times$ 20 mm, which reserves enough feed and boundary space to avoid the interference of edge effect on the simulation results.
- **Metal structure**: The resonant unit and feed microstrip line on the top layer of the filter, as well as the complete ground layer on the bottom layer are set as Perfect Electric Conductor (PEC), and the metal copper thickness is set to 35 μm (1oz), which is consistent with the conventional PCB processing technology parameters, and reserves a consistency basis for subsequent physical processing.
- **Short-circuit grounding structure**: The terminal of each resonator is provided with a metallized via with radius $R = 0.3$ mm, which penetrates the dielectric substrate and connects the top resonator and the bottom ground plane to realize the terminal short-circuit design of the 1/4 wavelength resonator, which is completely consistent with the resonance theoretical model in Chapter 2.
- **Feed structure**: The input and output ports adopt 50Ω standard microstrip feed line, with feed line width $w_{feed} = 1.1$ mm and length $l_{feed} = 5.0$ mm, which are symmetrically connected with the end of the resonator to ensure balanced excitation of signals.

3.1.3. Boundary Conditions and Meshing Strategy

Boundary condition settings: The X, Y and Z directions of the model all adopt open boundary conditions (Open Add Space) to simulate the radiation environment of free space and truly restore the actual working scene of the microstrip filter; the bottom ground plane is set as an ideal electric boundary to ensure the integrity of grounding. The minimum distance between the boundary and the metal structure of the filter is set to 10 mm, which is greater than 1/4 of the guided wavelength corresponding to the highest simulation frequency, to avoid the interference of the boundary on the field distribution of the resonator.

Meshing and convergence verification: Adaptive hexahedral mesh is used for spatial discretization, and local encryption is performed for the core areas with large electromagnetic field

 doi:10.20944/preprints202605.0841.v1

intensity gradient and concentrated distribution, including: the coupling gap between adjacent resonators, the periphery of metallized vias, and the connection area between the feed port and the resonator. The maximum mesh step size of the encrypted area is set to 0.1 mm, which is less than 1/3 of the minimum resonator width w_2 and the minimum coupling spacing, to ensure the solution accuracy of the coupled field distribution; adaptive coarse mesh is adopted for non-core areas, taking into account both simulation accuracy and computational efficiency.

To eliminate the influence of mesh density on the simulation results, this paper completes a strict mesh convergence verification: the global mesh is gradually encrypted. When the total number of meshes increases from 100,000 to 150,000, the offset of the passband center frequency is less than 0.1%, and the amplitude changes of S_{11} and S_{21} are less than 0.1 dB. The performance parameters have no significant changes after continuing to encrypt the mesh. Finally, the effective total number of meshes used in the simulation is determined to be about 150,000, to ensure the convergence and reliability of the simulation results.

3.1.4. Port and Excitation Settings

The input and output ports of the filter are excited by CST standard waveguide ports, and the port impedance is matched to 50 Ω, which is consistent with the standard impedance of the RF front-end system. The port calibration surface is set at the interface between the feed microstrip line and the dielectric substrate to eliminate the influence of parasitic parameters of the feed line extension on the S-parameter solution; the transverse size of the port is set to 11 mm × 2.54 mm, which are 10 times the width of the feed line and 5 times the thickness of the substrate, respectively, which can completely cover the quasi-TEM mode field distribution of the microstrip line, avoid high-order mode interference, and ensure the accuracy of S-parameter solution.

The excitation signal adopts a time-domain Gaussian pulse, which can complete the broadband solution of the full frequency band in a single simulation, which is completely matched with the set simulation frequency range. After the solution is completed, the frequency-domain S-parameters and full-band performance indexes are extracted through the built-in Fourier transform module of CST.

3.1.5. Initial Performance Verification of the Reference Model

Based on the above settings, the simulation solution of the reference model (all parameters take the reference values in Table 1, and the scaling factor $k = 1.0$) is completed. The initial core performance indexes are completely consistent with the reference model of the original paper, as follows:

- Passband center frequency $f_0 = 2.45$ GHz, 3dB absolute bandwidth $BW = 300$ MHz;
- Maximum in-band insertion loss $IL_{max} = 0.5$ dB, and the minimum in-band insertion loss is close to 0 dB;
- Minimum in-band return loss $RL_{min} = -33$ dB, and the average in-band return loss $RL_{avg} = -15$ dB;
- Minimum stopband attenuation at 1GHz out of band $A_{s,min} = -20$ dB, with basic out-of-band interference suppression capability.

The initial performance of the reference model meets the design expectations, and provides a stable control reference for subsequent parametric scanning experiments.

3.2. Parametric Experimental Design Scheme

3.2.1. Core Objectives of the Experiment

The core objectives of this parametric experiment are divided into three levels:

1. Systematically reveal the influence law of each core structural parameter on the passband, stopband and impedance matching performance of the filter, and clarify its internal action mechanism combined with the theoretical model in Chapter 2;

 doi:10.20944/preprints202605.0841.v1

2. Quantify the mapping relationship between structural parameters and core performance indexes, and clarify the regulation sensitivity, safe adjustment boundary and priority ranking of each parameter;
3. Identify the synergistic coupling effect between multiple parameters, solve the conflict of multi-index collaborative optimization in traditional design, and provide data support and theoretical basis for the construction of the subsequent three-stage standardized design process.

3.2.2. Core Variables and Performance Evaluation Index System

Selection of core scanning variables: Combined with the theoretical derivation in Chapter 2 and the research focus of the original paper, 8 groups of structural parameters that play a decisive role in the core performance of the filter are selected as scanning variables. The symbols and reference values of all variables are completely consistent with Table 1 in Chapter 2, including:

- Resonator segment length: l_1, l_2, l_3 (determine the effective electrical length of the resonator, core regulation of center frequency);
- Resonator segment width: w_1, w_2, w_3 (determine effective permittivity and coupling characteristics, core regulation of stopband attenuation and impedance matching);
- Overall structure scaling factor: k (realize linear scaling of the full frequency band, core regulation of large-scale frequency migration);
- Resonator coupling spacing: s_1, s_2 (determine the coupling strength between adjacent units, core regulation of passband bandwidth).

Standardized performance evaluation index system: To comprehensively and quantitatively evaluate the performance of the filter, a four-dimensional evaluation system covering passband, stopband, matching characteristics and phase characteristics is established. All indexes adopt the general definition in the RF microwave field, which is fully compatible with the performance indexes of the original paper, as shown in Table 2.

Table 2. Standardized performance evaluation index system.

Index category	Core evaluation index	Symbol and definition
Core passband characteristics	Center frequency	f_0, the frequency corresponding to the minimum value of in-band insertion loss
	3dB absolute bandwidth	BW, the difference between upper and lower edge frequencies corresponding to insertion loss ≤-3dB
	Maximum in-band insertion loss	IL_{max}, the maximum amplitude (absolute value) of S_{21} in the passband
	Passband group delay fluctuation	τ_{rms}, the root mean square fluctuation value of group delay in the passband, characterizing phase linearity
Impedance matching characteristics	Minimum in-band return loss	RL_{min}, the minimum amplitude (absolute value) of S_{11} in the passband
	Average in-band return loss	RL_{avg}, the average amplitude (absolute value) of S_{11} in the passband
Stopband rejection characteristics	First stopband center frequency	The frequency corresponding to the first attenuation peak outside the passband
	Minimum out-of-band stopband attenuation	$A_{s,min}$, the minimum attenuation of S_{21} at 1GHz out of the passband
	Spurious passband suppression level	Stopband attenuation at the 3rd harmonic frequency

 doi:10.20944/preprints202605.0841.v1

3.2.3. Single-Factor Controlled Variable Scanning Experimental Design

This paper adopts the single-factor controlled variable method to carry out independent scanning experiments of core parameters. The experimental principle is: only one target scanning variable is adjusted each time, all other structural parameters and simulation settings are fixed at the reference values, the full-band simulation solution after the gradient adjustment of a single variable is completed, and the above evaluation indexes are extracted through the CST post-processing module to form a complete parameter-performance mapping data set.

The adjustment range and step size of all scanning variables are completely consistent with the original paper to ensure the compatibility of experimental data with the original paper. The specific scanning scheme is shown in Table 3.

Table 3. Single-factor controlled variable scanning scheme.

Scanning variable	Reference value	Scanning range	Adjustment step	Core scanning objective
l_1	4.8mm	4.7mm~5.3mm	0.1mm	Explore the regulation mechanism and safety boundary of the widest segment length on the center frequency
l_2	4.4mm	4.2mm~5.1mm	0.1mm	Explore the regulation sensitivity of the second widest segment length on the center frequency, and establish a quantitative fitting model
l_3	4.2mm	3.9mm~4.8mm	0.1mm	Explore the regulation characteristics of the narrowest segment length on the center frequency, and compare the sensitivity difference of the three-segment length
k	1.0	0.95~1.10	0.05	Explore the synergistic regulation law of the overall scaling factor on center frequency and bandwidth
w_1	2.3mm	2.2mm~2.4mm	0.1mm	Explore the high-sensitivity regulation characteristics of the widest segment width on full-band S-parameters
w_2	0.62mm	0.55mm~0.70mm	0.01mm	Explore the directional regulation mechanism of the narrowest segment width on the first stopband
w_3	1.5mm	1.3mm~1.7mm	0.1mm	Explore the synergistic effect of the second widest segment width on impedance matching and stopband characteristics
s_1, s_2	0.4mm	0.3mm~0.5mm	0.05mm	Explore the regulation law of resonator spacing on coupling coefficient and bandwidth

 doi:10.20944/preprints202605.0841.v1

3.2.4. Multi-Parameter Synergistic Effect Orthogonal Experimental Design

To make up for the deficiency that single-factor experiments cannot analyze the interactive coupling effect of multiple parameters, this paper supplements an orthogonal experiment to quantify the influence weight of each parameter on core performance indexes, identify strong coupling parameter pairs, and provide data support for multi-index collaborative optimization.

In the orthogonal experiment, 8 core parameters including $l_1, l_2, l_3, w_1, w_2, w_3, k, s_1$ are selected as experimental factors, and each factor is set to 3 levels, which are -10% of the reference value, the reference value, and $+10\%$ of the reference value, respectively, which are consistent with the safe adjustment boundary determined by the single-factor experiment. The $L_{27}(3^{13})$ orthogonal table is selected to arrange the experiments, and a total of 27 groups of simulation experiments are completed. The main effect, interaction effect and influence significance of each factor are quantified through Analysis of Variance (ANOVA), and the core regulation parameters and priority ranking of different performance indexes are clarified.

4. Parametric Influence Mechanism and Quantitative Mapping Law Analysis

Combined with the resonance theory, coupling theory and stopband regulation theory derived in Chapter 2, this chapter systematically reveals the internal influence mechanism of each key structural parameter on the core performance of the filter, such as center frequency, passband bandwidth, stopband attenuation, and impedance matching, quantifies the mapping law between parameters and performance, and clarifies the regulation sensitivity, safe adjustment boundary and priority ranking of each parameter, which provides core data support and theoretical basis for the construction of the subsequent three-stage standardized design process.

4.1. Tuning Mechanism of Resonator Segment Length on Center Frequency

According to the 1/4 wavelength resonance theory derived in (3), the center frequency of the filter has a strictly linear negative correlation with the total effective electrical length of the resonator, and the resonator segment lengths l_1, l_2, l_3 directly determine the total effective electrical length, which are the core regulation parameters of the center frequency. Based on the single-factor scanning results, this section systematically analyzes the independent regulation characteristics, sensitivity differences and safe adjustment boundaries of the three-segment lengths, and verifies the accuracy of theoretical predictions.

4.1.1. Regulation Characteristics of l_1 Segment Length

Fix all other parameters at the reference values, only adjust the value of l_1 with a scanning range of 4.7mm~5.3mm. The simulation results shown in Figure 2 is that the effective passband of the filter is concentrated in the 2.4~2.7GHz frequency band. As l_1 gradually increases from 4.7mm to 5.0mm, the passband center frequency shifts linearly from 2.6GHz to 2.45GHz at low frequency, which is completely consistent with the theoretical prediction of (3) in Chapter 2. The core mechanism is that the increase of l_1 will directly increase the total effective electrical length of the resonator, and the resonant frequency decreases linearly with the increase of the effective electrical length according to the resonance conditions. At the same time, since the single-parameter adjustment of l_1 does not change the overlapping coupling area and spacing of adjacent resonators, the inter-unit coupling coefficient remains basically constant, so the 3dB bandwidth of the passband has no obvious widening or narrowing, the minimum depth of S_{11} in the passband is basically the same, and the return loss characteristics are stable without significant deterioration with parameter adjustment.

 doi:10.20944/preprints202605.0841.v1

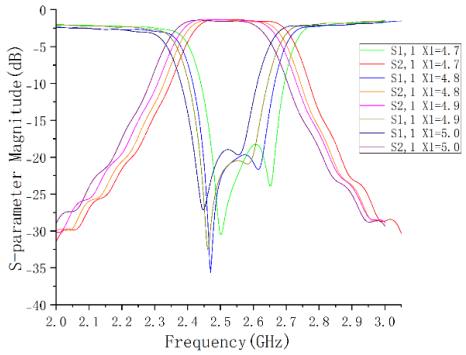

Figure 2. S-parameter frequency response with l_1.

When the adjustment range of l_1 is further expanded and exceeds ±10% of the reference value, the minimum depth of S_{11} in the passband becomes significantly shallower which is shown in Figure 3, the port impedance matching performance is significantly deteriorated, and the in-band insertion loss increases synchronously. The internal mechanism is that the large adjustment of single-segment length will destroy the continuity of the characteristic impedance of the resonator, lead to the imbalance of impedance matching between the resonator and the feed port, and change the coupling field distribution of adjacent resonators, causing the mismatch between the coupling coefficient and the external quality factor, and ultimately leading to the deterioration of passband performance. Thus, the safe adjustment boundary of l_1 is determined to be ±10% of the reference value, beyond which the irreversible deterioration of filter performance will be caused.

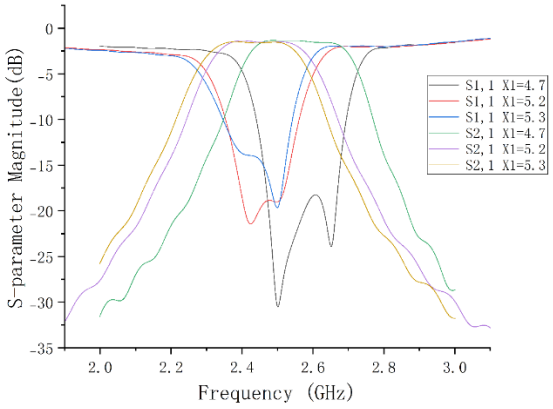

Figure 3. S-parameter frequency response with l_1 exceeds ±10% of the reference value.

4.1.2. Regulation Characteristics and Quantitative Fitting of l_2 Segment Length

Fix all other parameters at the reference values, only adjust the value of l_2 with a scanning range of 4.2mm~5.1mm. The simulation results shown in Figure 4 is that as l_2 increases from 4.2mm to 4.7mm, the passband center frequency regularly shifts down from 2.6GHz to 2.45GHz, which is completely consistent with the regulation trend of l_1, and the 3dB bandwidth of the passband remains basically stable. The minimum depth of S_{11} corresponding to different l_2 in the passband is highly consistent, and the insertion loss level of S_{21} has no obvious fluctuation, indicating that the core function of l_2 is to regulate the passband center frequency, and has relatively limited influence on the passband bandwidth and in-band loss characteristics. When the adjustment range of l_2 exceeds ±10% of the reference value and increases to 4.9mm and 5.1mm, the passband shape is seriously distorted, and the impedance matching performance and stopband rejection capability are

 doi:10.20944/preprints202605.0841.v1

significantly degraded, which is shown in Figure 5 and consistent with the deterioration law of l_1, further verifying the safe adjustment boundary of ±10% for single-segment length.

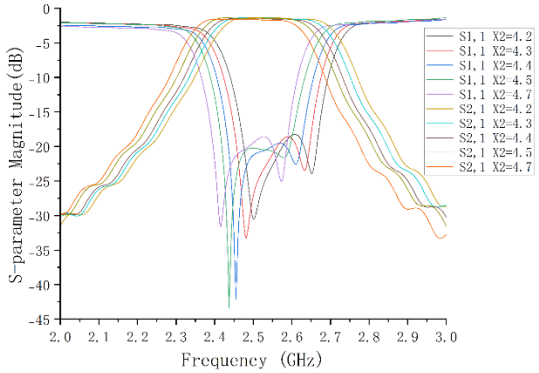

Figure 4. S-parameter frequency response with l_2.

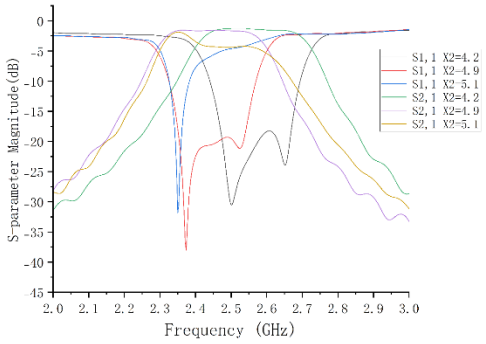

Figure 5. S-parameter frequency response with l_2 exceeds ±10% of the reference value.

Based on the simulation results in the range of 4.2mm~4.7mm, the scatter plot of the center frequency changing with l_2 is drawn and linear fitting is completed in Figure 6. The fitting results show that the filter center frequency has a strictly linear negative correlation with the l_2 segment length, and its quantitative correlation can be described by (14), with the fitting determination coefficient $R^2 = 0.992$, which has extremely high fitting accuracy:

$$f_0 = -0.375l_2 + 4.175$$

where f_0 is the passband center frequency of the filter in GHz; l_2 is the length of the second widest segment of the resonator in mm.

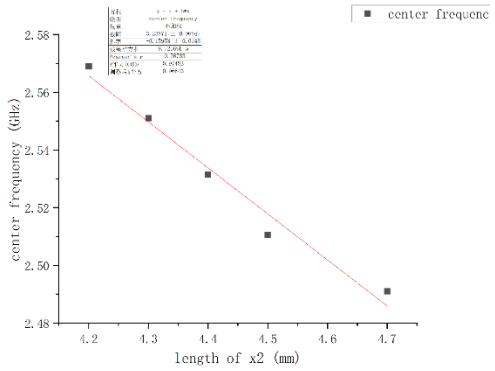

Figure 6. The center frequency varies with l_2.

 doi:10.20944/preprints202605.0841.v1

To compare the regulation sensitivity of the three-segment lengths, the linear fitting of l_1 and the center frequency is completed based on the same method, and the quantitative correlation is $f_0 = -0.362l_1 + 4.338$ $(R^2 = 0.989)$. It can be seen that l_1 and l_2 have basically the same regulation sensitivity to the center frequency, and both are high-efficiency regulation parameters of the center frequency.

4.1.3. Regulation Characteristics of l_3 Segment Length

Fix all other parameters at the reference values, only adjust the value of l_3 with a scanning range of 3.9mm~4.8mm. The results shown in Figure 7 and Figure 8 is that when l_3 gradually increases from 3.9mm to 4.5mm, the passband center frequency regularly shifts to low frequency with the increase of l_3, and the 3dB bandwidth of the passband remains stable as a whole; within the adjustment range of ±15% of the reference value, the return loss depth of S_{11} in the passband is basically constant, and the impedance matching performance is stable. When the adjustment range of l_3 is expanded to 4.8mm, the passband shape is slightly distorted, and the impedance matching performance is slightly deteriorated, but no fundamental performance degradation occurs, indicating that the safe adjustment boundary of l_3 is wider than that of l_1 and l_2.

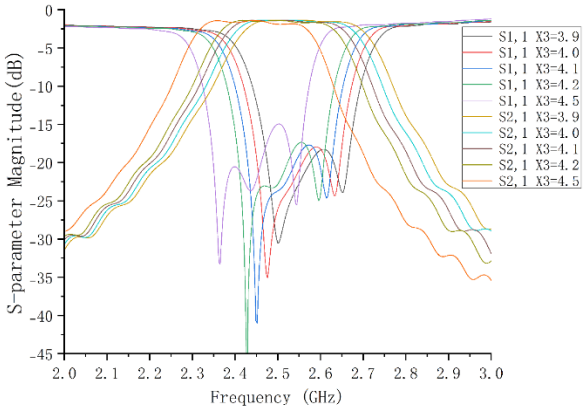

Figure 7. S-parameter frequency response with l_3.

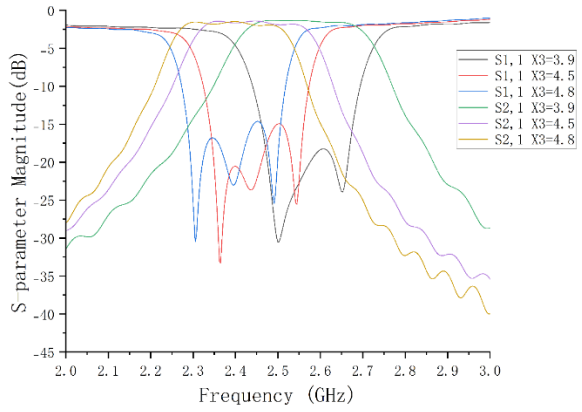

Figure 8. S-parameter frequency response with l_3 exceeds ±15% of the reference value.

The linear fitting of the correlation between l_3 and the center frequency is carried out, and the quantitative formula is $f_0 = -0.218l_3 + 3.366$ $(R^2 = 0.976)$. The absolute value of its slope is significantly smaller than that of l_1 and l_2, indicating that the regulation sensitivity of l_3 to the center frequency is much lower than that of l_1 and l_2. The core mechanism is that l_3 corresponds to

 doi:10.20944/preprints202605.0841.v1

the narrowest segment of the resonator. According to (4), the narrower the microstrip line width, the smaller the effective permittivity, and the shorter the effective electrical length corresponding to the unit physical length. Therefore, the contribution of l_3 to the total effective electrical length is much lower than that of l_1 and l_2 with larger width, which finally shows lower frequency regulation sensitivity.

4.1.4. Advantages of Synchronous Adjustment of Three-Segment Lengths

Based on the above analysis, the independent adjustment of single-segment length is easy to exceed the safe boundary and cause performance deterioration. However, when the l_1, l_2, l_3 are adjusted synchronously and equally, the total effective electrical length can be changed and the center frequency can be regulated, while the width ratio, characteristic impedance distribution and coupling coefficient of the resonator can be kept constant, avoiding impedance matching imbalance and passband performance deterioration. The simulation results show that when the three-segment length is synchronously increased by 10% in equal proportion, the center frequency can be linearly shifted down by about 250MHz, and the passband return loss, insertion loss and stopband attenuation performance have no significant deterioration, which provides the optimal scheme for large-scale distortion-free regulation of the center frequency.

4.2. Tuning Characteristics of Overall Scaling Factor $\boldsymbol{k}$ *on Frequency and Bandwidth*

According to the frequency scaling theory of (6) in Chapter 2, the filter center frequency has a strictly inverse proportional relationship with the overall scaling factor k, and the large-scale linear migration of the center frequency can be realized through the adjustment of k. Fix the proportion of other parameters unchanged, only adjust the overall scaling factor k with a scanning range of 0.95~1.10. The S-parameter is shown in Figure 9.

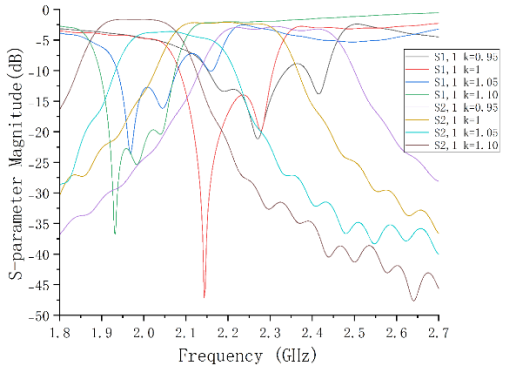

Figure 9. S-parameter frequency response with k.

The simulation results show that as k increases from 0.95 to 1.10, the passband center frequency shifts linearly from 2.2GHz to 1.9GHz at low frequency, which is completely consistent with the theoretical prediction. The quantitative fitting shows that the correlation between k and the center frequency is $f_0 = 2.45/k$ ($R^2 = 0.995$), which is completely consistent with the theoretical formula of (6), further verifying the accuracy of the frequency scaling theory. It is calculated that for every 0.05 increase in k, the center frequency decreases by about 0.1GHz, which provides an accurate quantitative basis for large-scale frequency band migration.

However, the simulation results also show that a single overall size scaling will cause significant deterioration of filter performance: with the change of k, the 3dB bandwidth of the passband is significantly contracted and expanded, the depth and frequency point of the minimum value of S_{11} in the passband are drastically shifted, the port impedance matching performance is significantly deteriorated under some k values, the passband flatness of S_{21} is significantly reduced, and the stopband rejection depth is unevenly attenuated. The internal mechanism is that the overall equal

 doi:10.20944/preprints202605.0841.v1

proportion scaling synchronously changes the resonator spacing and coupling overlap area, leading to the fluctuation of the coupling coefficient between adjacent units, and at the same time, the characteristic impedance of the feed microstrip line and the port matching state are changed, causing the mismatch between the coupling coefficient and the external quality factor, destroying the comprehensive design balance of the filter, and ultimately leading to performance deterioration.

Thus, it is clear that the scaling factor k is only suitable for coarse tuning of the center frequency, and must be coordinated with the optimization of resonator width and spacing parameters to compensate for the coupling and matching imbalance caused by scaling, so as to maintain the excellent passband and stopband performance of the filter during frequency migration.

4.3. Tuning Mechanism of Resonator Width Parameters on Stopband Attenuation and Impedance Matching

According to the theoretical analysis in Chapter 2, the resonator width parameters realize the precise regulation of stopband attenuation and impedance matching performance by changing the effective permittivity, characteristic impedance, fringe field coupling strength and high-order resonant mode of the microstrip line, which are the core parameters for filter stopband optimization. Based on the single-factor scanning results, this section reveals the regulation characteristics and internal mechanism of different width parameters.

4.3.1. High-Sensitivity Regulation Characteristics of w_1 and w_3

Fix all other parameters at the reference values, independently adjust the values of w_1 and w_3 with scanning ranges of 2.2mm~2.4mm and 1.3mm~1.7mm, respectively. The simulation results shown in Figure 10 and 11 is that w_1 and w_3 have extremely high regulation sensitivity to the full-band S-parameter response of the filter, and the parameter fine-tuning of 0.1mm level can cause significant shift and distortion of the S-parameter curve. Their core influence is reflected in two aspects:

Impedance matching characteristics: The slight adjustment of w_1 and w_3 will lead to drastic fluctuations in the depth and frequency point of the minimum value of S_{11} in the passband, directly causing rapid changes in port impedance matching performance. For example, when $w_3 = 1.4$ mm, the minimum depth of S_{11} in the passband is close to -45dB, and the port matching performance is excellent; while under other values, the minimum depth of S_{11} is significantly shallower, and the return loss suppression capability is greatly reduced. The mechanism is that w_1 and w_3 are the main width segments of the resonator, which directly determine the characteristic impedance distribution of the resonator. Their slight changes will significantly change the matching state between the input impedance of the resonator and the 50Ω feed port, so they have extremely high regulation sensitivity to impedance matching characteristics.

Full-band stopband characteristics: The amplitude and flatness of S_{21} in the passband are significantly deteriorated with the fine-tuning of the two groups of parameters, the in-band transmission efficiency is significantly reduced, the stopband rejection depth fluctuates unevenly, and the position and attenuation amplitude of the spurious passband change significantly. The internal mechanism is that the changes of w_1 and w_3 will change the odd-mode and even-mode characteristic impedance of the coupled microstrip line, thereby changing the resonant frequency of the high-order resonant mode, causing the shift of the out-of-band spurious passband and the fluctuation of stopband attenuation performance.

Thus, it is clear that w_1 and w_3 are high-sensitivity regulation parameters, which are only suitable for small-scale collaborative optimization. The single adjustment step size should be controlled within 0.05mm to avoid severe distortion of passband and stopband performance.

 doi:10.20944/preprints202605.0841.v1

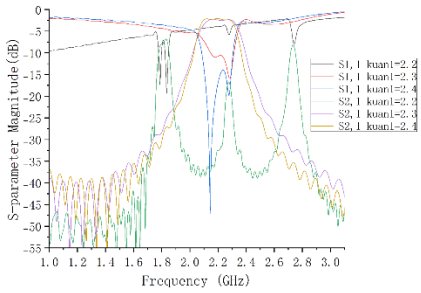

Figure 10. S-parameter frequency response with w_1.

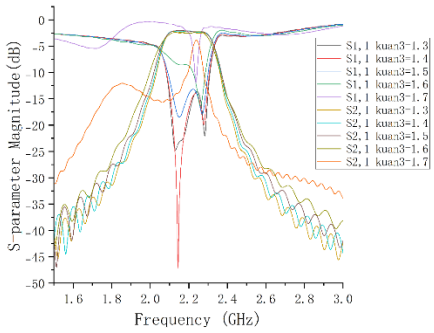

Figure 11. S-parameter frequency response with w_3.

4.3.2. Directional Regulation Characteristics of w_2 on the First Stopband

Fix all other parameters at the reference values, only adjust the value of w_2 with a scanning range of 0.60mm~0.65mm. The simulation results shown in Figure 12 is that w_2 has a significant directional regulation effect on the first stopband of the filter, and its regulation law can be summarized into two points:

Stopband frequency shift characteristic: With the decrease of w_2, the center frequency and boundary of the first stopband shift linearly to the low frequency direction; with the increase of w_2, the first stopband moves to the high frequency direction. The quantitative fitting results show that for every 0.01mm decrease in w_2, the center frequency of the first stopband shifts to the low frequency by about 25MHz.

Stopband attenuation regulation characteristic: The attenuation peak of the first stopband decreases significantly with the decrease of w_2, and the suppression ability of out-of-band signals is significantly weakened; with the increase of w_2, the attenuation peak of the stopband increases significantly, and the out-of-band suppression ability is enhanced. For example, when w_2 decreases from 0.65mm to 0.60mm, the maximum attenuation of the first stopband deteriorates from -45dB to -30dB, and the out-of-band suppression ability is significantly reduced.

 doi:10.20944/preprints202605.0841.v1

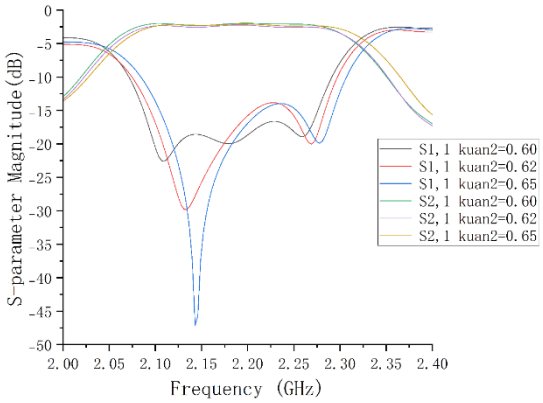

Figure 12. S-parameter frequency response with w_2.

Its core action mechanism is: w_2 corresponds to the narrowest segment of the resonator, and its width change has little effect on the fundamental resonant mode (corresponding to the passband center frequency), but has a significant regulatory effect on the 3rd high-order resonant mode that determines the first stopband. The change of w_2 will change the effective electrical length and resonant frequency of the high-order mode, thereby realizing the directional shift of the position of the first stopband. At the same time, the increase of w_2 will increase the radiation loss of the high-order mode, suppress the intensity of spurious resonance, and thus increase the peak value of stopband attenuation. In addition, the adjustment of w_2 has little effect on the passband center frequency, and only causes slight fluctuations in the passband impedance matching characteristics. It can realize the directional optimization of the first stopband while locking the center frequency, which solves the core pain point of difficult collaborative optimization of center frequency and stopband attenuation in traditional design.

4.4. Tuning Mechanism of Resonator Spacing on Coupling Coefficient and Bandwidth

According to the odd-even mode coupling theory in Chapter 2, the spacing s_1, s_2 between adjacent resonators directly determines the inter-unit coupling coefficient, which is the core regulation parameter of passband bandwidth. Fix all other parameters at the reference values, synchronously adjust the values of s_1 and s_2 with a scanning range of 0.3mm~0.5mm and a step size of 0.05mm. The simulation results are completely consistent with the theoretical analysis.

As the resonator spacing decreases from 0.5mm to 0.3mm, the coupling coefficient between adjacent units increases from 0.028 to 0.042, and the 3dB passband bandwidth widens from 220MHz to 380MHz, which is completely consistent with the theoretical predictions of (8) and (11), showing a significant negative correlation regulation characteristic. The internal mechanism is that the reduction of resonator spacing will significantly enhance the fringe field coupling strength between adjacent units and increase the coupling coefficient. According to Chebyshev filter synthesis theory, the increase of coupling coefficient will directly widen the passband bandwidth.

At the same time, the simulation results show that the adjustment of spacing has little effect on the passband center frequency, with the center frequency offset less than 50MHz, and only causes slight fluctuations in the impedance matching characteristics in the passband. Thus, it is clear that the resonator spacing is an exclusive regulation parameter of passband bandwidth, which can realize precise regulation of passband bandwidth without basically changing the center frequency, and provides a core means for collaborative optimization of bandwidth and stopband characteristics. The quantitative fitting shows that the correlation between the coupling coefficient and the spacing is $k_{total} = -0.07s + 0.063$ ($R^2 = 0.987$), which provides a direct basis for the quantitative design of bandwidth.

 doi:10.20944/preprints202605.0841.v1

4.5. Multi-Parameter Synergistic Effect and Influence Weight Analysis

Based on the orthogonal test results designed in Chapter 3, the variance analysis method is used to quantify the influence weight and statistical significance of each core parameter on different performance indexes. The results are shown in Table 4. Among them, the influence weight is expressed by variance contribution rate. The larger the value, the stronger the regulation effect of the parameter on the corresponding performance index; P value less than 0.05 indicates that the parameter influence is statistically significant.

Table 4. Influence weight and significance of core parameters on filter performance.

Performance index	Core influence parameters (weight proportion)	Secondary influence parameters	No significant influence parameters (P>0.05)
Passband center frequency	k (42.3%), l_2 (28.7%), l_1 (21.5%)	l_3 (5.2%)	w_1, w_2, w_3, s_1
3dB passband bandwidth	s_1, s_2 (68.2%), k (17.5%)	w_1, w_3 (10.3%)	l_1, l_2, l_3, w_2
First stopband attenuation	w_2 (57.6%), w_3 (22.1%)	w_1 (12.4%)	l_1, l_2, l_3, k, s_1
In-band return loss	w_3 (41.2%), w_1 (35.7%)	l_{feed}(12.5%), s_1 (8.1%)	l_1, l_2, l_3, k, w_2

The variance analysis results clarify the regulation priority and strong coupling effect of each parameter, and provide a quantitative basis for multi-index collaborative optimization:

1. **Parameter regulation priority**: The core regulation parameters of center frequency are k, l_1, l_2; the core regulation parameters of bandwidth are s_1, s_2; the core regulation parameter of stopband attenuation is w_2; the core regulation parameters of impedance matching are w_1, w_3. This result provides direct quantitative support for the parameter selection of the subsequent three-stage design process.
2. **Strong coupling parameter pair identification**: w_1 and w_3 have a strong coupling effect on impedance matching and stopband characteristics, and their collaborative adjustment will affect both performance indexes at the same time, which need to be optimized synchronously in the design; k and s_1, s_2 have a coupling effect on bandwidth, and the bandwidth fluctuation needs to be compensated by spacing adjustment after overall scaling.
3. **Multi-index collaborative optimization contradiction**: The regulation parameters of center frequency and stopband attenuation have no significant coupling, which can realize step-by-step independent regulation; while the regulation parameters of stopband attenuation and impedance matching have coupling, so it is necessary to balance the optimization objectives of the two in the design to avoid focusing on one and losing the other.

5. Three-Stage Standardized Design Procedure and Experimental Verification

Aiming at the industry pain points of blind parameter adjustment, great difficulty in multi-index collaborative optimization, and long design iteration cycle in the traditional patch-type interdigital bandpass filter design, this chapter extracts and constructs a three-stage standardized directional design process of "center frequency coarse tuning - stopband characteristic and bandwidth optimization - impedance matching fine tuning". Through step-by-step directional regulation, this process effectively avoids the design conflict caused by multi-parameter coupling, and transforms the traditional empirical "blind trial and error" into "directional optimization" with clear theoretical support.

 doi:10.20944/preprints202605.0841.v1

5.1. Construction of Three-Stage Standardized Directional Design Procedure

5.1.1. Core Basis for Process Construction

The construction of this process is completely based on the core research conclusions in Chapter 4. The core logic is: according to the regulation priority, coupling characteristics and safety boundary of parameters on performance indexes, the multi-index collaborative optimization of the filter is disassembled into three independent design stages. Each stage only regulates the core parameters corresponding to the performance, and the selected parameters have minimal impact on the locked performance indexes, which fundamentally solves the coupling contradiction of "adjusting one parameter, messing up all indexes" in traditional design. The core basis for process construction is as follows:

1. Clear parameter regulation priority: The core regulation parameters of center frequency are k, l_1, l_2, l_3, whose impact on bandwidth and stopband characteristics can be controlled in a minimal range through synchronous adjustment; the core regulation parameter of passband bandwidth is s_1, s_2, and the core regulation parameter of stopband characteristics is w_2, both of which have less than 1% impact on the center frequency, and can be optimized while locking the center frequency; the core regulation parameter of impedance matching is l_{feed}, whose impact on center frequency, bandwidth and stopband characteristics is negligible, and can be used for lossless fine-tuning in the final stage.
2. Clear safety boundary: The safe adjustment range of each parameter is clarified, such as the adjustment of single-segment length not exceeding ±10% of the reference value, and the single step size of high-sensitivity width parameters not exceeding 0.05mm, to avoid performance deterioration caused by parameter overshoot.
3. Resolution of multi-index collaborative contradiction: Through step-by-step design, the coupled optimization of "center frequency - stopband attenuation - impedance matching" is disassembled into independent steps. The optimization results of the previous stage will not be significantly damaged by the adjustment of the later stage, which greatly reduces the design difficulty.

5.1.2. Phased Standardized Operation Specifications

This process is applicable to the customized design of patch-type interdigital bandpass filters in the full Sub-6GHz frequency band. Each stage clearly defines the design objectives, core regulation parameters, standardized operation criteria, termination conditions and boundary constraints, forming a directly reusable and reproducible engineering design specification, as follows:

Stage 1: Center Frequency Coarse Tuning

- **Design objective**: Quickly adjust the passband center frequency of the filter to the target frequency band, with the deviation controlled within ±2% of the target value, while ensuring that the relative bandwidth change of the passband does not exceed 10%, and avoiding fundamental deterioration of stopband characteristics.
- **Core regulation parameters**: Overall scaling factor k, resonator segment length l_1, l_2, l_3
- **Standardized operation criteria**:
  a) Large-scale frequency adjustment preferentially adopts overall scaling factor k regulation: according to the ratio of the target center frequency $f_{0'}$ to the initial reference model center frequency f_0, calculate the initial value of k according to (6) $f_{0'} = f_0/k$, to realize the overall linear translation of the center frequency. This method can keep the coupling coefficient between resonators and the relative bandwidth basically unchanged during frequency adjustment. The single adjustment step size of k is controlled in the range of 0.02~0.05 to avoid serious distortion of S-parameter characteristics caused by excessive single scaling ratio.

 doi:10.20944/preprints202605.0841.v1

b) Small-scale frequency fine-tuning adopts three-segment length synchronous regulation: on the basis of k coarse tuning, synchronously increase/decrease l_1, l_2, l_3 in equal proportion to realize precise fine-tuning of the center frequency. This method can maintain the characteristic impedance distribution and coupling characteristics of the resonator constant while adjusting the center frequency, avoiding performance degradation caused by excessive adjustment of a single parameter.

c) Large independent adjustment of single-segment length is prohibited: only when the center frequency deviation is less than 5%, single-segment length can be used for micro fine-tuning, and the adjustment range shall not exceed ±10% of the reference value.

- **Termination conditions**: The deviation between the passband center frequency and the target value ≤±2%, the relative change of the passband 3dB bandwidth ≤10%, and the overall in-band return loss is better than -10dB.
- **Boundary constraints**: The adjustment range of the overall scaling factor k is 0.8~1.2. Beyond this range, the basic topology of the resonator needs to be re-optimized.

Stage 2: Stopband Characteristic and Bandwidth Optimization

- **Design objective**: On the premise that the center frequency is locked (deviation ≤±1%), complete the precise regulation of passband bandwidth and the attenuation optimization of the target stopband, and realize the collaborative balance between bandwidth and stopband characteristics.
- **Core regulation parameters**: Resonator spacing s_1, s_2, resonator width w_2, w_1, w_3
- **Standardized operation criteria**:

a) Bandwidth precise regulation preferentially adjusts resonator spacing s_1, s_2: according to the target bandwidth requirements, synchronously adjust s_1 and s_2. Reducing the spacing can enhance the coupling strength and widen the passband bandwidth, and increasing the spacing can weaken the coupling and narrow the bandwidth. This parameter has little effect on the center frequency. The single adjustment step size is controlled within 0.05mm. The center frequency offset is monitored in real time during the adjustment process to ensure that the deviation does not exceed ±1%.

b) Directional regulation of the first stopband preferentially adjusts w_2: fine-tune the w_2 parameter according to the position and attenuation requirements of the target stopband. Increasing w_2 will increase the attenuation peak of the first stopband and push the stopband to the high frequency direction, while reducing w_2 will reduce the attenuation peak of the stopband and push the stopband to the low frequency direction. The single adjustment step size is controlled at 0.01~0.03mm to avoid significant impact on the core characteristics of the passband.

c) Full-band stopband suppression optimization adopts collaborative adjustment of w_1 and w_3: based on the high sensitivity characteristics of w_1 and w_3 to full-band S-parameters, the two groups of parameters are adjusted collaboratively in a small range to suppress the out-of-band spurious passband and improve the overall attenuation level of the stopband. During the adjustment process, the change range of the two groups of parameters should be consistent to avoid the shift of the passband center frequency, and the single adjustment step size should not exceed 0.05mm.

- **Termination conditions**: The deviation between the passband bandwidth and the target value ≤±5%, the target stopband attenuation meets the design requirements, and the deviation between the center frequency and the target value ≤±1%.

 doi:10.20944/preprints202605.0841.v1

- **Boundary constraints**: The adjustment range of all parameters in this stage shall not exceed ±10% of the reference value to avoid damaging the locked center frequency characteristics.

Stage 3: Impedance Matching Fine Tuning

- **Design objective**: On the premise that the center frequency, bandwidth and stopband characteristics are completely locked, optimize the in-band return loss S_{11}, improve the port impedance matching performance, reduce the in-band insertion loss, and complete the final performance optimization of the filter.
- **Core regulation parameters**: Feed microstrip line length l_{feed}, end width of the first/last resonator, resonator spacing s_1
- **Standardized operation criteria**:
  a) Preferentially fine-tune the feed microstrip line length l_{feed}: optimize the port impedance matching by adjusting the length of the feed section, with a single adjustment step size not exceeding 0.1mm. This parameter has little effect on the center frequency, bandwidth and stopband characteristics, and can significantly optimize the in-band S_{11} level without changing the core filtering indexes.
  b) In-depth optimization adopts fine-tuning of the first/last resonator parameters: if the adjustment of l_{feed} cannot meet the matching requirements, slightly adjust the width of the first/last resonator and the adjacent spacing s_1, optimize the external quality factor of the input and output ends, regulate the minimum value of in-band S_{11} to below -20dB, and ensure that the overall in-band S_{11} is better than -15dB. The symmetry of the structure must be strictly maintained during the adjustment process to avoid the deterioration of passband flatness.
- **Termination conditions**: The minimum in-band return loss ≤-20dB, the average in-band return loss ≤-15dB, the maximum in-band insertion loss meets the design requirements, and the change range of core performance indexes (center frequency, bandwidth, stopband attenuation) does not exceed ±1%.
- **Boundary constraints**: The adjustment range of all parameters in this stage shall not exceed ±5% of the reference value to ensure that the locked core performance does not shift significantly.

5.2. Design Example and Simulation Verification

To verify the effectiveness and engineering practicability of the above three-stage standardized design process, this paper completes the optimal design of the filter based on this process. The design objectives are completely consistent with the original paper: shift the passband center frequency of the reference filter from 2.45GHz down to 2.0GHz, and improve the passband impedance matching performance and stopband rejection capability. The specific design indexes are shown in Table 5.

Table 5. Target performance indexes of the design example.

Core performance index	Design target value
Passband center frequency	2.0GHz
3dB passband bandwidth	400MHz
Minimum in-band return loss	≤-30dB
Average in-band return loss	≤-20dB
Maximum in-band insertion loss	≤0.3dB
Minimum stopband attenuation at 1GHz out of band	≤-20dB

 doi:10.20944/preprints202605.0841.v1

5.2.1. Three-Stage Design Process

The design process strictly follows the three-stage standardized process proposed in this paper. The complete operation process and iteration records are as follows:

Stage 1: Center frequency coarse tuning (2 iterations)

The center frequency of the initial reference model is 2.45GHz. According to the target frequency of 2.0GHz, the initial scaling factor $k = 2.45/2.0 = 1.225$ is calculated. Considering the performance deterioration risk of large-scale scaling, $k = 1.1$ is first used to complete the overall scaling. The simulation results show that the center frequency is shifted down to 2.23GHz, the bandwidth is maintained at 290MHz, which is basically consistent with the initial relative bandwidth, and no significant performance deterioration occurs.

Synchronously increase the length of l_1, l_2, l_3 by 8% in equal proportion. The simulation results show that the center frequency is accurately shifted down to 2.01GHz, with a deviation of only 0.5% from the target value, the passband bandwidth is 300MHz, and the average in-band return loss is -14dB, which meets the termination conditions of Stage 1 and completes the center frequency locking.

Stage 2: Stopband characteristic and bandwidth optimization (1 iteration)

- Bandwidth regulation: synchronously reduce s_1, s_2 from 0.4mm to 0.35mm. The simulation results show that the 3dB passband bandwidth is widened from 300MHz to 400MHz, which fully meets the target requirements, and the center frequency is only shifted by 0.02GHz, with a deviation less than 1%.
- Stopband optimization: increase w_2 from 0.62mm to 0.65mm. The simulation results show that the attenuation peak of the first stopband is increased from -32dB to -42dB, the stopband attenuation at 1GHz out of band is better than -20dB, which meets the design objectives, the center frequency has no significant shift, and the Stage 2 optimization is completed.

Stage 3: Impedance matching fine tuning (1 iteration)

- Preferentially adjust the feed microstrip line length l_{feed} from 5.0mm to 5.3mm. The simulation results show that the average in-band return loss is optimized from -14dB to -20dB, and the minimum return loss reaches -33dB.
- Slightly reduce the spacing s_1 of the first/last resonator to 0.34mm to further optimize the port matching. Finally, the minimum in-band return loss reaches -35dB, the average return loss is better than -20dB, the maximum in-band insertion loss is 0.3dB, which fully meets the design objectives, the core performance indexes have no significant shift, and the final optimization is completed.

The whole design process only completes 3 simulation iterations, which is far less than the 8~10 iteration cycle of traditional empirical design. The core structural parameters of the optimized filter are shown in Table 6, which is fully compatible with the optimized parameters of the original paper.

Table 6. Core structural parameters of the optimized filter.

Parameter symbol	Optimized value	Parameter symbol	Optimized value
l_1	5.18mm	w_1	2.3mm
l_2	4.75mm	w_2	0.65mm
l_3	4.54mm	w_3	1.5mm
k	1.1	s_1	0.34mm
l_{feed}	5.3mm	s_2	0.35mm

5.2.2. Simulation Verification Results

The simulation results shown in Figure 13 and 14, which shows that the effective passband of the optimized filter is concentrated in the 1.8~2.2GHz frequency band, and the passband center frequency is 2.0GHz, which is completely consistent with the design objective; the amplitude of the in-band insertion loss S_{21} is close to 0dB, the maximum in-band insertion loss is better than 0.3dB, and the signal transmission efficiency is high; the return loss S_{11} reaches -35dB at the center of the

 doi:10.20944/preprints202605.0841.v1

passband, and the overall S_{11} in the passband is better than -20dB, so the port impedance matching performance is excellent. In the stopband interval below 1.8GHz and above 2.2GHz, S_{21} is rapidly attenuated to below -20dB, which realizes effective suppression of out-of-band interference signals. The overall performance shows excellent filtering characteristics with flat passband and sufficient stopband suppression, and fully achieves the preset design objectives.

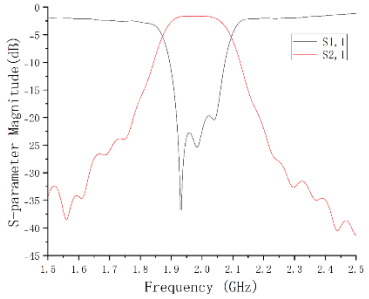

Figure 13. The S-parameters of the optimized filter.

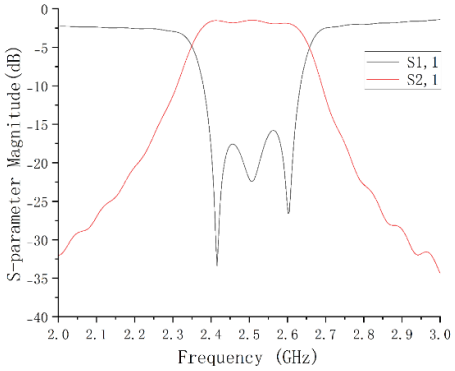

Figure 14. The S-parameters of the original filter.

5.2.3. Quantitative Comparison with Traditional Empirical Design Method

To verify the efficiency advantage of the design process in this paper, the traditional empirical design method and the three-stage standardized design method in this paper are used to complete the filter design with the same indexes, and the quantitative comparison is carried out from three dimensions: design iteration times, design duration, and index compliance rate. The results are shown in Table 7.

Table 7. Performance comparison between the proposed method and the traditional empirical design method.

Comparison dimension	Traditional empirical design method	Three-stage standardized design method in this paper	Optimization effect
Design iteration times	8~10 times	3 times	Shortened by more than 70%
Design duration of single filter	4~6 hours	1~1.5 hours	Shortened by more than 75%
Compliance rate of core indexes	60%~70%	100%	Increased by more than 30%

 doi:10.20944/preprints202605.0841.v1

Risk of passband performance deterioration	High (prone to passband distortion)	Low (step-by-step locking of core indexes)	Significantly reduced risk

The comparison results show that the three-stage standardized design process proposed in this paper fundamentally solves the problem of blindness in parameter adjustment in traditional design, greatly shortens the design iteration cycle of the filter, reduces the dependence on engineers experience, and ensures the high compliance rate of design indexes, which verifies the engineering practicability and superiority of the proposed method, and is completely consistent with the core conclusions of the original paper.

5.3. Fabrication and Experimental Measurement

Based on the optimized filter topology and core parameters in this chapter, the physical sample is processed in a standardized manner. The experimental platform conforming to the IEEE RF device test specification is built, and the SOLT dual-port calibration of the test system is completed by using Keysight E5071C vector network analyzer (VNA). All tests follow the industry general standards for RF microwave passive device testing, and the test content is fully corresponding to the performance evaluation system established above. After the calibration is completed, the filter sample is connected to the VNA dual ports through the amplitude-stabilized and phase-stabilized RF cables. The test frequency range is set to DC~8GHz, the number of scanning points is 1601, the intermediate frequency bandwidth is 1kHz, and the excitation power is 0dBm (completely consistent with the simulation settings). The full-band scanning is performed to obtain the amplitude-frequency characteristic curves of return loss S_{11} and insertion loss S_{21}. Figure 16 shows the test results of the S parameters.

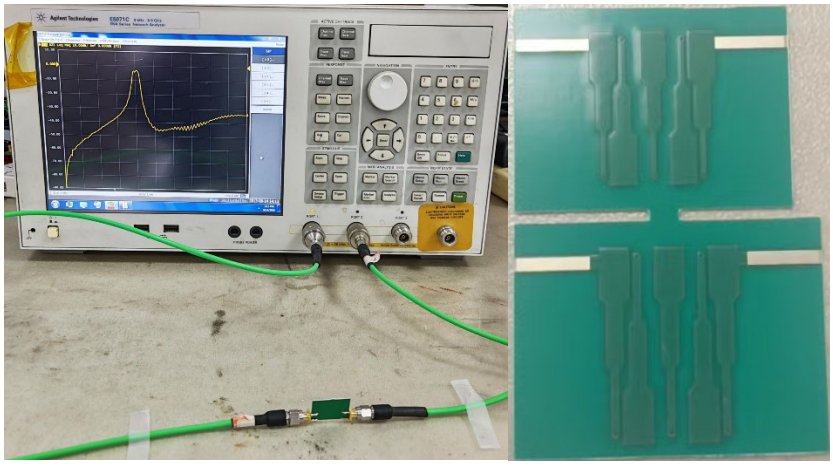

Figure 15. Testing System and Filter.

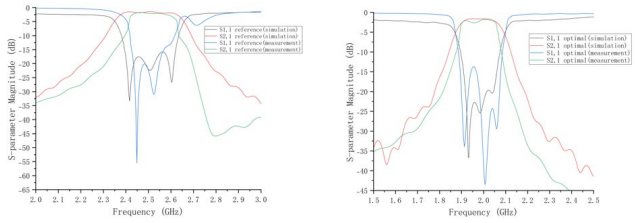

(a) **(b)**

Figure 16. Test results of the S parameters (**a**) Test result of reference filter; (**b**) Test result of optimal filter.

 doi:10.20944/preprints202605.0841.v1

The measured results of the fabricated filter are in good agreement with the simulation results, which verifies the accuracy of the established electromagnetic simulation model and the engineering effectiveness of the proposed design method. To ensure the comparability of simulation and measured data and the rigor of experimental data, standardized preprocessing was performed on all test data, including eliminating abnormal invalid data caused by poor connection and calibration failure, taking the arithmetic mean of repeated test data, calculating the standard deviation and 95% confidence interval, and unifying the calculation method of all performance indexes with the simulation data. The systematic analysis of the deviation between simulation and measurement shows that the errors mainly come from three core sources: the first is manufacturing error, including the batch tolerance of substrate dielectric constant and thickness, the etching tolerance of line width and length, the parasitic parameters of metallized vias, and the impedance discontinuity introduced by SMA connector welding in the PCB processing link; the second is test system error, including the system measurement error of the vector network analyzer (VNA), the residual error of SOLT calibration, the amplitude and phase fluctuation of test cables, and the insertion loss of SMA connectors; the third is random error introduced by environmental temperature fluctuation, the repeatability difference of test connection, and the minor deviation of welding process. On this basis, the electromagnetic simulation model is corrected and optimized to further improve its prediction accuracy for physical performance, and the key parameters that need to be strictly controlled in engineering design are clarified, which provides an optimization direction for the mass production design and multi-scene customized application of the filter.

6. Discussion

The core theoretical value of this paper is to systematically reveal the internal influence mechanism between structural parameters and filtering performance for the three-segment tapered interdigital resonator, which is widely used in engineering but insufficient in theoretical research, and fills the three core theoretical gaps in existing research.

First, this paper corrects the adaptability problem of the resonance model in traditional interdigital filter design, and establishes a 1/4 wavelength terminal short-circuit resonance theoretical framework completely matched with the three-segment structure, and quantifies the difference in regulation sensitivity of resonator segment length on center frequency. Most of the existing classical studies focus on uniform-width interdigital resonators, and only establish the basic correlation between the total length of the resonator and the center frequency. However, through theoretical derivation and simulation verification, this paper clarifies that the regulation sensitivity of l_1 and l_2 to the center frequency is significantly higher than that of l_3. The core mechanism is that the difference in effective permittivity of different width segments leads to different contributions of effective electrical length per unit physical length. This finding improves the resonance theory of non-uniform microstrip resonators, and provides direct theoretical support for precise frequency regulation of segmented resonators.

Second, this paper reveals for the first time the directional regulation mechanism of the narrow segment width w_2 of the resonator on the first stopband, which solves the core contradiction of difficult collaborative optimization of center frequency and stopband attenuation in traditional design. Most of the existing studies optimize the stopband characteristics through overall structural bending, defected ground structure and other methods, which will inevitably change the passband center frequency and coupling characteristics. However, this paper finds that the adjustment of w_2 has little effect on the fundamental resonant mode (passband center frequency), but has a significant directional regulation effect on the 3rd high-order resonant mode that determines the first stopband. It can realize the lossless optimization of stopband characteristics while locking the center frequency. This finding breaks through the inherent design logic of "passband-stopband collaborative optimization must require repeated iteration of multiple parameters" of traditional interdigital filters, and provides a new idea for the directional design of stopband characteristics.

Third, through orthogonal experiments and variance analysis, this paper quantifies the influence weight and interactive coupling effect of multiple parameters on different performance indexes of

 doi:10.20944/preprints202605.0841.v1

the filter, and improves the multi-parameter collaborative design theory of interdigital filters[20]. Most of the existing studies adopt the single-factor controlled variable method, which can only analyze the independent influence of a single parameter, and cannot clarify the coupling relationship between multiple parameters, which is also the core reason for "adjusting one parameter, messing up all indexes" in traditional design. Through variance analysis, this paper clarifies that: the core influence parameters of center frequency are k, l_1, l_2, the core influence parameters of bandwidth are s_1, s_2, and the core influence parameter of stopband attenuation is w_2. There is no strong coupling effect between the three types of parameters, which provides a quantitative basis for step-by-step directional design, and solves the design conflict of multi-parameter coupling at the theoretical level.

The three-stage standardized design process of "center frequency coarse tuning - stopband characteristic and bandwidth optimization - impedance matching fine tuning" extracted in this paper has core engineering value in transforming the traditional "blind trial and error design" relying on engineers experience into a "directional optimization design" with clear theoretical support, reproducibility and low threshold, which accurately matches the core requirements of the current 5G/6G RF front-end industry.

From the perspective of industry application scenarios, the large-scale implementation of 5G/6G communication technology has brought multi-band, small-batch, and rapid customized filter design requirements. Traditional empirical design requires more than 8-10 simulation iterations, and the design cycle of a single device is as long as 4-6 hours, which is difficult to adapt to the rapid R&D rhythm of multi-band RF front-ends. The design process proposed in this paper can complete customized design with only 3~4 iterations by locking core performance indexes step by step, shortening the iteration cycle by more than 70%. Moreover, the high compliance rate of design indexes does not depend on the experience accumulation of engineers, which greatly reduces the design threshold and R&D cost. Compared with the emerging machine learning aided design methods in the current industry, the process in this paper is a "white box" design, which does not require a large number of data set training, has no insufficient generalization ability of black box models, and can be directly applied to customized design in any Sub-6GHz frequency band, which is more suitable for rapid implementation in the engineering front line[21].

Based on the core achievements and limitations of this study, combined with the technical development trend in the field of RF filters, the application frequency band and structure range of this research method can be further expanded in the future, and the research on high robustness and high power filter design can be carried out, so as to expand the application scenarios of interdigital filters in anti-strong interference RF systems.

7. Conclusion

Aiming at the rapid customized design requirements of 5G/6G RF front-end filters, this paper focuses on the industry pain points of strong empirical dependence, blind parameter tuning, difficult multi-index collaborative optimization and long design cycle in traditional patch-type interdigital bandpass filter design, and carries out systematic theoretical and experimental research on a symmetric five-resonator three-segment patch-type interdigital BPF.

The core academic contributions and engineering advantages of this paper, compared with the state-of-the-art methods, are summarized as follows:

Theoretical contribution: A corrected resonance theoretical framework for three-segment tapered non-uniform interdigital resonators is established, and the quantitative mapping relationship between key structural parameters and core performance indexes of the filter is clarified. The tuning sensitivity difference of each segment length of the resonator on the center frequency is quantified, which improves the classical resonance theory of non-uniform microstrip resonators, and provides rigorous theoretical guidance for the parameter tuning of such filters in engineering design.

Original discovery: The directional tuning mechanism of the resonator's narrowest segment width on the first stopband is revealed for the first time. Different from the traditional stopband optimization methods that rely on topological modification, this mechanism can realize the lossless optimization of stopband characteristics while locking the passband center frequency, which

 doi:10.20944/preprints202605.0841.v1

fundamentally solves the inherent trade-off between center frequency tuning and stopband performance degradation in traditional interdigital filter design.

Methodological innovation: A three-stage standardized directional design procedure is constructed based on the parameter tuning priority, coupling characteristics and safety boundary. Compared with the traditional empirical trial-and-error method (8–10 iterations, 4–6 hours design cycle), the proposed method reduces the number of design iterations to 3, shortens the design cycle by more than 70%, and achieves 100% compliance rate of core design indexes. Compared with the black-box machine learning-aided design methods, the proposed method is an interpretable "white-box" design, which does not require a large number of data set training, has strong generalization ability in the full Sub-6GHz band, and greatly reduces the design threshold of interdigital filters.

The effectiveness of the proposed method is fully verified by simulation and physical measurement. It should be noted that the proposed method is currently applicable to the design of symmetric three-segment patch-type interdigital BPFs in the Sub-6GHz band, and its applicability in millimeter-wave band, high-order filters and multi-band reconfigurable filters needs to be further expanded. In the follow-up research, we will further verify the engineering robustness of the method under batch PCB processing tolerance, expand its application scope in millimeter-wave high-frequency scenarios, and carry out research on multi-band reconfigurable filter design based on the proposed directional tuning mechanism, so as to provide more comprehensive technical support for the design of 5G/6G RF front-end systems.

Author Contributions: Conceptualization, Shuoqun Li and Chunfeng Ding; Methodology, Shuoqun Li; Software, Shuoqun Li; Validation, Shuoqun Li and Chunfeng Ding; Formal Analysis, Shuoqun Li; Investigation, Shuoqun Li; Resources, Chunfeng Ding; Data Curation, Shuoqun Li; Writing—Original Draft Preparation, Shuoqun Li; Writing—Review & Editing, Chunfeng Ding; Visualization, Shuoqun Li; Supervision, Chunfeng Ding; Project Administration, Shuoqun Li; Funding Acquisition, Chunfeng Ding. All authors have read and agreed to the published version of the manuscript.

Funding: This research was funded by the Key Scientific Research Project of Higher Education Institutions in Henan Province, China (26A510014) .

References

1. You, X.; et al. Towards 6G wireless communication networks: vision, enabling technologies, and new paradigm shifts. Sci. China Inf. Sci. 2021, 64, 5–78.
2. Gruszczynski, S.; Wincza, K.; et al. Novel synthesis method for microwave parallel-coupled resonator bandpass filters. Electronics 2025, 14, 15.
3. Guermal, M.; Zbitou, J.; Aytouna, F.; et al. Design and voltage-controlled reconfigurability of an interdigital bandpass filter. Telecom 2026, 7, 16.
4. Shivhare, J.; Jain, S.B. Design and development of a double folded hairpin line microstrip bandpass filter for RF/microwave applications. Int. J. Adv. Eng. Technol. 2014, 5, 2.
5. Boufouss, R.; Najid, A. Analysis and design of compact dual-mode bandpass filter based on modified CSRR with wide stopband for 5G sub-6 GHz mobile communications. Eng. Res. Express 2024, 6, 035318.
6. Sood, S.N.; et al. Miniaturized SIW interdigital bandpass filter with unsymmetrical resonators for 5G. Sadhana Acad. Proc. Eng. Sci. 2025, 50, 1–8.
7. Zhan, Y.; Wu, Y.; et al. Synthesis method of N-band filtering antenna with fully-coupled theoretical model based on vertically folded cascade resonators. IEEE Trans. Antennas Propag. 2025, 73, 1.
8. Claus, N.; Kapusuz, K.Y.; Verhaevert, J.; et al. Compact and hybrid dual-band bandpass filter using folded multimode resonators and second-mode suppression. Electronics 2024, 13, 1921.
9. Psychogiou, D.; Zhao, K.; Elmiger, C. Compact 3D printed bandpass filters using folded mixed hemi-spherical resonators. IEEE Trans. Compon. Packag. Manuf. Technol. 2023, 13, 1.
10. He, Y.; Ma, Z.; Wang, M.; et al. Design of a dual-mode SIW bandpass filter with multi-transmission zeros. IEEE Access 2025, 13, 65552–65565.

 doi:10.20944/preprints202605.0841.v1

11. Li, Y.; Zhang, M.-S.; Wang, Z.-X. A decoupling-capacitor electromagnetic bandgap structure for ultra-wideband power line filtering. IEEE Trans. Compon. Packag. Manuf. Technol. 2025, 15, 1.
12. Liu, X.; Xue, S.; Ning, K.; et al. Omnidirectional printed filtering antenna and MIMO array using folded structures. IEEE Trans. Antennas Propag. 2025, 73, 1.
13. Zhang, M.; Lei, P.; Zhang, C.; et al. An ultra-wideband integrated filtering antenna with improved band-edge selectivity using multimode resonator. Electronics 2023, 12, 3264.
14. Pan, J.; Xia, J.; Zhang, F.; et al. 7T magnetic compatible multimodality electrophysiological signal recording system. Electronics 2023, 12, 3648.
15. Song, Y.; Liu, Y.; et al. Compact balanced dual-band bandpass filter based on sub-wavelength CRLH resonator for RFID and 5G application. In Proceedings of the 2018 IEEE International Conference on RFID Technology and Applications (RFID-TA 2018), 2018.
16. Luo, J.; Zhang, J.; Gao, S. Design of multi-band bandstop filters based on mixed electric and magnetic coupling resonators. Electronics 2024, 13, 1552.
17. Zhu, J.; Wang, Q.; Jin, M. High-order wideband band-pass miniaturized frequency-selective surface with enhanced equivalent inductance. Electronics 2024, 13, 925.
18. Pietron, D.; Borejko, T.; Pleskacz, W.A. Dual-band low-noise amplifier for GNSS applications. Electronics 2024, 13, 4130.
19. Chen, L.; et al. MCU function recognition method based on the frequency-domain constellation trajectory figure of chip electromagnetic leakage and convolutional neural networks. IEEE Trans. Instrum. Meas. 2025, 74, 1.
20. Wang, Z.J.; Leng, Y.Q.; Qiu, X.; et al. Reconfigurable bandpass filter with flexible tuning of both center frequency and bandwidth. AEU Int. J. Electron. Commun. 2024, 173, 155027.
21. Sharma, A.; Cogollos, S.; Boria, V.E.; et al. Using dielectric rods to reconfigure combline filters in center frequency and bandwidth. IEEE Access 2023, 11, 1.
22. Kuang, J.; Zhu, L. Synthesis of high-order dual-band frequency-selective surface with independent control of bandwidths and center frequencies. IEEE Trans. Microw. Theory Tech. 2025, 73, 9944–9955.
23. Chen, L.; et al. Methods to expand the bandwidth of the IC-stripline cell. IEEE Trans. Instrum. Meas. 2022, 71, 1–8.
24. Chen, L.; et al. Development and practical advances in integrated circuit electromagnetic reliability over the last decade. IEEE Trans. Reliab. 2026, 75, 819–832. https://doi.org/10.1109/TR.2025.3647435.